Available online at www.sciencedirect.com
SCIENCE DIRECT
International Journal of Mass Spectrometry 254 (2006) 155–162
International Journal of Mass Spectrometry
www.elsevier.com/locate/ijms

Exploration of the catalytic oxidation of ethylene with N_2O mediated by atomic alkaline-earth metal cations

Andrea Dašić, Xiang Zhao, Diethard K. Bohme *

Department of Chemistry, Centre for Research in Mass Spectrometry and Centre for Research in Earth and Space Science, York University, Toronto, Ont., Canada M3J 1P3

Available online 8 June 2006

Abstract

The catalytic oxidation of ethylene by N_2O mediated by atomic alkaline-earth metal cations has been investigated both experimentally and theoretically. An ICP/SIFT tandem mass spectrometer was employed to measure the kinetics and product distributions of the reactions of $CaO^{\bullet+}$, $SrO^{\bullet+}$ and $BaO^{\bullet+}$ with ethylene. Together with previous measurements of the kinetics of the oxidation reactions of $Ca^{\bullet+}$, $Sr^{\bullet+}$ and $Ba^{\bullet+}$ with N_2O, these results allow an evaluation of the catalytic oxidation of ethylene by these atomic cations via O-atom transfer. Potential energy surfaces were explored with $Ca^{\bullet+}$ as a catalyst using density functional theory for the formation of three possible isomers of oxidized ethylene: acetaldehyde, ethylene oxide and ethenol.

Keywords: Ion catalysis; Alkaline-earth metal cations; Ethylene; O-atom transport; N_2O reduction

1. Introduction

The Wacker or Hoechst–Wacker process is one of the first examples of an organometallic catalysis applied on an industrial scale; ethylene is oxidized to acetaldehyde using palladium(II) chloride and copper(II) chloride as catalysts under an oxygen atmosphere [1]. However, this process has now fallen somewhat out of favor and demand for acetaldehyde has dropped because of the expensive technology that is required [2]. The availability of low-cost process technology would re-stimulate the demand for this molecule which is an important precursor for the commercial-scale manufacture of acetic acid, ethanol, ethyl acetate, maleic acid, etc. [3] and an important intermediate in the synthesis of dyes, pharmaceuticals, perfumes and pesticides [4].

Here we report experimental and theoretical results for catalytic cycles that proceed in the gas phase and that also oxidize ethylene but with atomic metal radical cations as catalysts. The catalytic cycle is shown in Fig. 1. The oxidant of choice is N_2O and the catalysts of choice are atomic radical cations of the alkaline-earth metals Ca, Sr and Ba. Beryllium and magnesium were not included because of instrumental limitations with light atomic ions.

The "thermodynamic window of opportunity" [5] for the catalytic formation of acetaldehyde is determined by the O-atom affinities of N_2 (to form N_2O), $OA(N_2) = 40\,kcal\,mol^{-1}$ [6], and the O-atom affinities of C_2H_4 (to form acetaldehyde), $OA(C_2H_4) = 113\,kcal\,mol^{-1}$ [6]. This means that the O-atom affinity of the catalyst, $OA(M^{\bullet+})$, must have an intermediate value, $40\,kcal\,mol^{-1} < OA(M^{\bullet+}) < 113\,kcal\,mol^{-1}$. The O-atom affinities of $Ca^{\bullet+}$, $Sr^{\bullet+}$ and $Ba^{\bullet+}$ meet this thermodynamic requirement since $OA(Ca^{\bullet+}) = 78.9\,kcal\,mol^{-1}$, $OA(Sr^{\bullet+}) = 81.1\,kcal\,mol^{-1}$ and $OA(Ba^{\bullet+}) = 103.2\,kcal\,mol^{-1}$ [6].

We have measured previously the efficiency of the oxidations of $Ca^{\bullet+}$, $Sr^{\bullet+}$ and $Ba^{\bullet+}$ with N_2O [5]. Additional measurements are reported here for the kinetics of the reactions of $CaO^{\bullet+}$, $SrO^{\bullet+}$ and $BaO^{\bullet+}$ with C_2H_4. Also, computations have been achieved with $Ca^{\bullet+}$ as a catalyst that elucidate the mechanisms of the two catalytic steps and provide a complete potential energy landscape for the overall catalysis to produce acetaldehyde. The calculations are extended to the catalytic formation of two other neutral products that are both isomers of acetaldehyde: ethylene oxide and ethenol.

A number of gas-phase studies in the past have addressed the oxidation of ethylene by transition metal oxide ions [7]. Some

* Corresponding author. Tel.: +1 416 736 2100x66188; fax: +1 416 736 5936.
E-mail address: dkbohme@yorku.ca (D.K. Bohme).

1387-3806/$ – see front matter © 2006 Elsevier B.V. All rights reserved.
doi:10.1016/j.ijms.2006.05.002

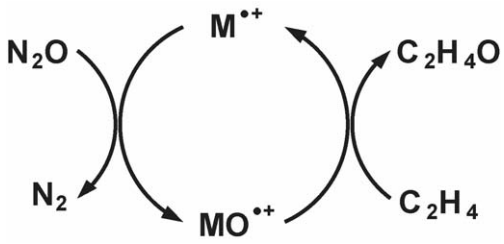

Fig. 1. Generalized catalytic cycle for the homogeneous oxidation of ethylene by nitrous oxide, mediated by atomic metal cations.

have considered the reverse reactions of bare metal ions with ethylene oxide [8], but none have demonstrated the catalytic activity of alkaline-earth metal cations in the gas-phase oxidation of ethylene.

2. Methods

2.1. Experimental methods

The reactions were investigated with an inductively coupled plasma/selected-ion flow tube (ICP/SIFT) tandem mass spectrometer. The ICP/SIFT instrument has been described in detail previously [9]. Elemental ions of interest are generated in argon plasma operating at atmospheric pressure and ca. 5500 K. Diluted solutions containing the metal salt of interest having concentration of ca. 5 $\mu g\,l^{-1}$ were peristaltically pumped via nebulizer into the plasma. The ions were then mass selected by a quadrupole mass filter, and injected into flowing He carrier gas at 0.35 ± 0.01 Torr and 295 ± 2 K. After experiencing about 10^5 collisions with He atoms, the ions were allowed to react with added nitrous oxide. N_2O was added directly into the flow tube and the atomic-oxide cations were produced. Ethylene was introduced further downstream in the reaction region where it reacted with the atomic oxide cations. Reactant and product ions were sampled with a second quadrupole mass spectrometer and were measured as a function of added reactant. Reaction rate coefficients were derived from the linear semilogarithmic decays of $MO^{\bullet+}$ in the usual way using pseudo-first-order kinetics [10]. It is important to point out that neutral products are not detected in these experiments but can often be inferred from known thermodynamics.

To avoid the addition of N_2O into the flow tube for the formation of atomic oxide cations, we have modified our instrument to also allow generation of atomic-oxide cations prior to the Q0 region of the upstream quadrupole mass filter. N_2O now can also be introduced just after the skimmer cone by adding it through a 10 micron capillary with flows of 25–35 ml min^{-1}. Metal oxide ions that are produced in this region by reactions with incoming atomic ions are mass selected by a quadrupole mass filter and then introduced into the flow tube. We were successful using this technique in the generation of $SrO^{\bullet+}$ and $BaO^{\bullet+}$, but signals for $CaO^{\bullet+}$ were too small. A modification also has been made downstream, after the sampling nose cone: the single quadrupole detector used previously has been replaced with a triple quadrupole mass spectrometer prototype API 4000.

All measurements using both ICP/SIFT and ICP/SIFT/QqQ instruments were performed at a room temperature of 295 ± 3 K. The helium buffer gas pressure was 0.35 ± 0.01 Torr. The nitrous oxide and ethylene were obtained commercially and were of high purity (Matheson Gas products, >98.0% and >99.5%, respectively).

2.2. Computational methods

Density functional theory (DFT) was applied to the study of the reactions $Ca^{\bullet+} + N_2O \rightarrow CaO^{\bullet+} + N_2$ and $CaO^{\bullet+} + C_2H_4 \rightarrow Ca^{\bullet+} + (2C,4H,O)$ for all three isomers of the oxidation product, as well as the reaction $N_2O + C_2H_4 \rightarrow N_2 + CH_3CHO$. All DFT calculations were carried out using the Gaussian 98, Revision A.11.4 package [11]. Geometries of reactants, intermediates, transition states, and products were fully optimized at the level of B3LYP [12] exchange-correlation functional using 6-311++G(d,p) basis set. Analytical harmonic vibrational frequencies were computed at the same level of theory to obtain the zero-point energies and to characterize the nature of the optimized structures. All minima (all real frequencies) and transition state (one imaginary frequency) structures were verified. The connection between points on the potential energy surface was verified using the intrinsic reaction coordinate (IRC) procedure as implemented in Gaussian 98, and developed by Gonzales and Schleger [13]. All reaction enthalpies, including the barrier heights of transition states, are calculated with respect to the total energy of the reactants. Cartesian coordinates and electronic energies for all optimized structures are available in the Supplementary Material.

3. Experimental results and discussion

3.1. Oxidation reactions of $M^{\bullet+}$ with N_2O

$Ca^{\bullet+}$, $Sr^{\bullet+}$ and $Ba^{\bullet+}$ cations have been found previously in our laboratory to abstract an O atom cleanly from N_2O according to Eq. (1) with rate coefficients of 1.6×10^{-10} cm^3 $molecule^{-1}$ s^{-1}, 6.3×10^{-11} cm^3 $molecule^{-1}$ s^{-1}, and 2.4×10^{-10} cm^3 $molecule^{-1}$ s^{-1}. N-atom transfer did not compete with O-atom transfer:

$$M^{\bullet+} + N_2O \rightarrow MO^{\bullet+} + N_2 \quad (1)$$

3.2. Reduction reactions of $MO^{\bullet+}$ with C_2H_4

$CaO^{\bullet+}$, $SrO^{\bullet+}$ and $BaO^{\bullet+}$ were all observed to react rapidly with ethylene, $k \geq 2 \times 10^{-10}$ cm^3 $molecule^{-1}$ s^{-1}. The four product channels (2a) to (2d) were observed with all three of these oxide cations. Fig. 2 displays the measured ion profiles.

$$MO^{\bullet+} + C_2H_4 \rightarrow M^{\bullet+} + (C_2H_4O) \quad (2a)$$

$$MO^{\bullet+} + C_2H_4 \rightarrow M^{+}(C_2H_3O) + H^{\bullet} \quad (2b)$$

$$MO^{\bullet+} + C_2H_4 \rightarrow MOH^{+} + C_2H_3^{\bullet} \quad (2c)$$

$$MO^{\bullet+} + C_2H_4 \rightarrow MO^{\bullet+}(C_2H_4) \quad (2d)$$

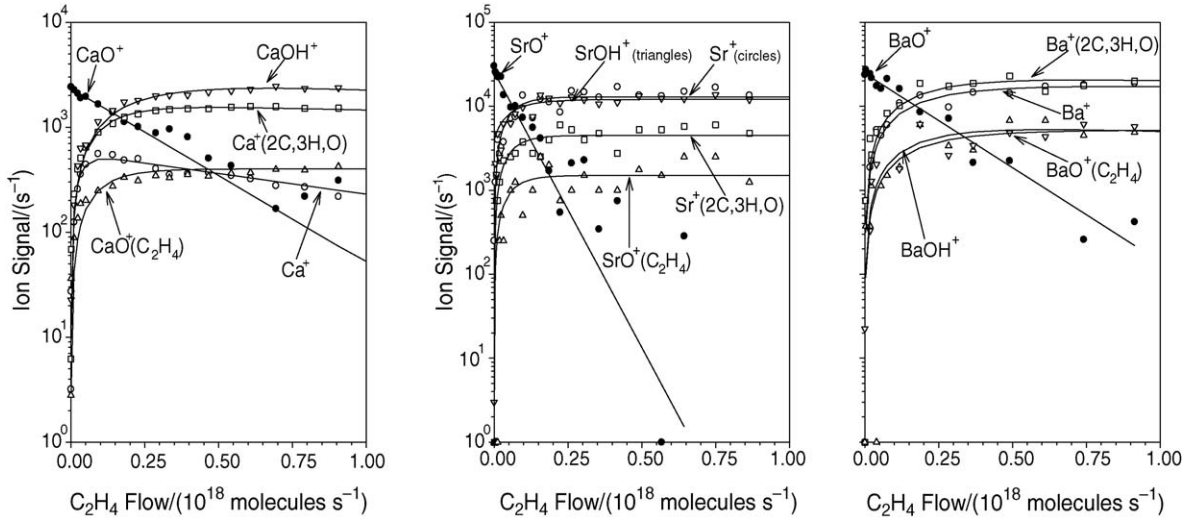

Fig. 2. Ion profiles recorded for the chemistry initiated by $CaO^{\bullet+}$, $SrO^{\bullet+}$, and $BaO^{\bullet+}$ with ethylene at 295 ± 3 K in helium buffer gas at 0.35 Torr. N_2O is present in the $CaO^{\bullet+}$ experiment (1.9×10^{18} molecule s^{-1}) but not in the $SrO^{\bullet+}$ and $BaO^{\bullet+}$ experiments in which $MO^{\bullet+}$ was generated before the first selection quadrupole.

Channel (2a) involves O-atom transfer and is the second step in the catalytic cycle of interest. Channel (2b) involves H-atom elimination with the formation of an organometallic cation of unknown structure while channel (2c) corresponds to H-atom transfer with formation of a hydroxide cation. Channel (2d) corresponds to addition and is likely to involve collisional stabilization with He. Fig. 2 shows data obtained. Table 1 provides a summary of the measured rate coefficients and product distributions.

Table 1 shows that each oxide cation has its own preferred product channel(s): hydroxide formation (2c) with $CaO^{\bullet+}$, O-atom transfer (2a) with $SrO^{\bullet+}$, and H-atom elimination (2b) and O-atom transfer (2a) with $BaO^{\bullet+}$.

O-atom transfer (2a) with $CaO^{\bullet+}$ and $SrO^{\bullet+}$ is exothermic for the formation of acetaldehyde as well as ethylene oxide and ethenol. The known O-atom affinities are 78.9 ± 4.4, 81.1 ± 4.6, and 103.2 ± 1.6 kcal mol^{-1} for $Ca^{\bullet+}$, $Sr^{\bullet+}$, and $Ba^{\bullet+}$, respectively [6], and the O-atom affinities of ethylene for the formation of acetaldehyde, ethylene oxide, and ethenol are 112.9, 84.7 and 102.7 kcal mol^{-1}, respectively [6]. In comparison, O-atom transfer from $BaO^{\bullet+}$ to ethylene is exothermic for the formation of acetaldehyde (by 10 kcal mol^{-1}), endothermic for the formation of ethylene oxide (by 18 kcal mol^{-1}) and thermoneutral for the formation of ethenol. This implies that acetaldehyde is the preferred neutral product in the reaction with $BaO^{\bullet+}$. Since the enthalpy of formation of acetaldehyde is the lowest of the three isomers, the formation of CH_3CHO will be the most exothermic channel with all three metal oxide cations and therefore the most favorable.

Table 1
Rate coefficients[a] and product distributions[b] measured for reactions of alkaline-earth oxide cations with ethylene, reaction (2), proceeding in helium at 295 ± 3 K and 0.35 ± 0.01 Torr

	$MO^{\bullet+}$		
	$CaO^{\bullet+}$	$SrO^{\bullet+}$	$BaO^{\bullet+}$
k	$\geq 2.0 \times 10^{-10}$[c]	1.0×10^{-9}	2.8×10^{-10}
k_c[d]	1.2×10^{-9}	1.1×10^{-9}	1.0×10^{-9}
k/k_c	≥ 0.17	0.91	0.28
(2a)	0.18	0.43	0.35
(2b)	0.16	0.15	0.43
(2c)	0.62	0.37	0.10
(2d)	0.04	0.05	0.12

[a] k is the measured total reaction rate coefficient in units of cm^3 $molecule^{-1}$ s^{-1} and has an estimated uncertainty of less than ± 30%.
[b] The product ratio is estimated to be accurate to less than ± 20%.
[c] Measured in the presence of N_2O and so the occurrence of the catalytic cycle in the reaction region.
[d] k_c is the collision rate coefficient calculated using the algorithm of the modified variational transition-state/classical trajectory theory developed by Su and Chesnavich [14].

The H-atom elimination channel (2b), although minor in the reactions with $CaO^{\bullet+}$ and $SrO^{\bullet+}$, is the major channel in the reaction with $BaO^{\bullet+}$. Perhaps Ba^+(2C,3H,O) has special stability. We are exploring separately the nature of the possible organometallic ions that may be formed in this channel.

Channel (2c) shows a clear trend of decreasing importance down the column of the periodic table. H atom transfer is exothermic in all cases, $D(C_2H_3\text{-}H) = 110.6 \pm 1.0$ kcal mol^{-1} [6], and the trend in importance may follow a trend in decreasing exothermicity because of the decreasing H-atom affinity of $MO^{\bullet+}$. The available H-atom affinities [6] are 124.2 ± 27.2, 132.6 ± 9.2, and 124.1 ± 6.2 kcal mol^{-1} for $CaO^{\bullet+}$, $SrO^{\bullet+}$, and $BaO^{\bullet+}$, respectively, but these are too uncertain to be definitive about the trend in exothermicity. We have therefore computed the energies, $HA(MO^{\bullet+})$, for the dissociation of the alkaline-earth metal hydroxides ($MOH^+ \rightarrow MO^{\bullet+} + H^\bullet$) at B3LYP level of theory with SDD basis set used for the metal and 6-311++G(d,p) for oxygen and hydrogen. The computed enthalpies of dissociation are given in Table 2 along with the experimental values. With the exception of $HA(MgO^{\bullet+})$, the computations indicate a clear decrease in $HA(MO^{\bullet+})$ going down the group. The computed values are lower than experiment for $BeO^{\bullet+}$ and $MgO^{\bullet+}$, but

Table 2
HA($MO^{\bullet+}$) in kcal mol^{-1} at 298 K for alkaline-earth metal oxide radical cations

$MO^{\bullet+}$	Theory	Experiment[a]
$BeO^{\bullet+}$	142.7	160.1 ± 9.2
$MgO^{\bullet+}$	124.4	134.4 ± 7.6
$CaO^{\bullet+}$	135.0	124.2 ± 27.2
$SrO^{\bullet+}$	132.2	132.6 ± 9.2
$BaO^{\bullet+}$	128.2	124.1 ± 6.2

[a] From Ref. [6].

agree with experiment for $CaO^{\bullet+}$, $SrO^{\bullet+}$ and $BaO^{\bullet+}$ within the experimental uncertainty.

Channel (2d) is the minor channel and expected to proceed by collisional stabilization with He as the third body. The branching ratio for this channel is quite insensitive to the nature of $MO^{\bullet+}$ but this is difficult to rationalize since our calculations (see below) have shown several minima in the potential energy surface for this channel so that the exact nature of the adduct ion cannot be specified. The well depth of these minima will depend on the nature of the metal as will the potential energy surfaces for the competing bimolecular channels.

4. Theoretical results and discussion

4.1. Oxidation of $Ca^{\bullet+}$ with Nitrous Oxide

We considered the lowest doublet state potential energy surface for the reaction of $Ca^{\bullet+}$ (a doublet) with the N_2O molecule (a singlet). Both end-on and side-on approaches have been investigated and the complete surface is shown in Fig. 3.

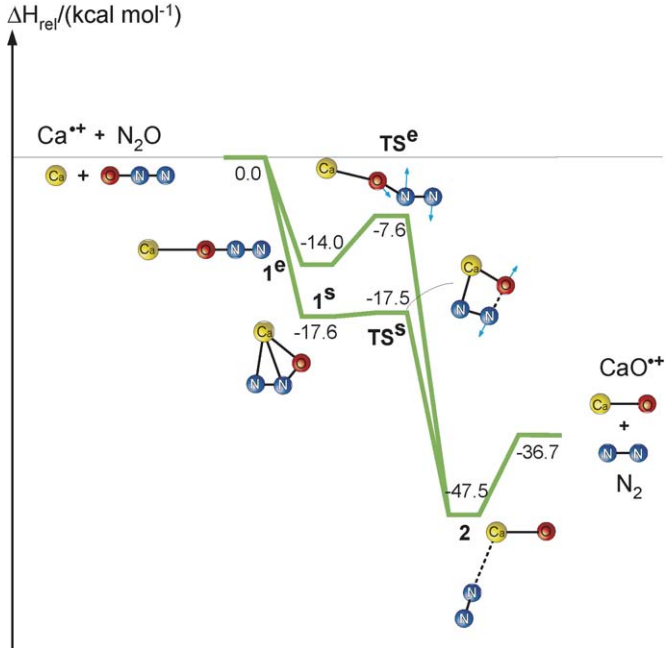

Fig. 3. Potential energy surface for the reaction of $Ca^{\bullet+}$ with N_2O to form $CaO^{\bullet+}$ and N_2. Relative enthalpies are computed at the B3LYP/6-311++G(d,p) level of theory.

The optimized geometries are illustrated in Fig. 1 and absolute energies are listed in Table 3 in the Supplementary Material.

4.1.1. End-on approach

A collinear approach was chosen in which $Ca^{\bullet+}$ interacts end-on with O in N_2O ($\angle CaON \approx 180^\circ$) and forms the reactant complex $\mathbf{1}^e$. The O atom is then transferred over an energy barrier (TS^e) and this forms the product complex **2** that dissociates into the final products. In the intermediate $\mathbf{1}^e$ a new bond is formed, Ca–O (2.340 Å). Both O–N and N–N bonds are slightly shorter; O–N by 0.003 Å (1.200 Å), and N–N bond by 0.022 Å (1.114 Å) then respective bonds in N_2O (1.203 and 1.136 Å).

4.1.2. Side-on approach

$Ca^{\bullet+}$ can also approach the central nitrogen atom in N_2O and form the reactant complex $\mathbf{1}^s$. The energies of this complex and the transition state TS^s are more than 17 kcal mol^{-1} below the energy of the initial reactants and lower than the energies of the intermediate $\mathbf{1}^e$ and the transition state TS^e.

We would expect $Sr^{\bullet+}$ and $Ba^{\bullet+}$ to show similar energy profiles for the O-atom abstraction from N_2O because they also have s^1 valence electron configurations.

4.2. Oxidation of ethylene by $CaO^{\bullet+}$

According to the available O-atom affinities, oxidation of ethylene by $CaO^{\bullet+}$ is exothermic for the formation of three isomers: acetaldehyde, ethylene oxide and ethenol (vinyl alcohol), as indicated in Eq. (5). Formation of acetaldehyde:

$$CaO^{\bullet+} + C_2H_4 \rightarrow Ca^{\bullet+} + CH_3CHO,$$
$$\Delta_r H^\circ = -34.0 \pm 4.7\ \text{kcal mol}^{-1} \quad (5a)$$

$$CaO^{\bullet+} + C_2H_4 \rightarrow Ca^{\bullet+} + CH_2CH_2O,$$
$$\Delta_r H^\circ = -5.7 \pm 4.4\ \text{kcal mol}^{-1} \quad (5b)$$

$$CaO^{\bullet+} + C_2H_4 \rightarrow Ca^{\bullet+} + CH_2CHOH,$$
$$\Delta_r H^\circ = -23.8 \pm 4.4\ \text{kcal mol}^{-1} \quad (5c)$$

is the most exothermic.

Our calculations show that initial formation of an intermediate $(CaOC_2H_4)^{\bullet+}$ is common to the ultimate formation of all three neutral product isomers and so is presented first.

4.2.1. Formation of $(CaOC_2H_4)^{\bullet+}$

The nearly side-on approach of $CaO^{\bullet+}$ to CH_2CH_2 is included in the potential energy surface shown in Fig. 4 and formation of a covalent O–C bond is found to be a two-step process. An electrostatically bound "side-on" adduct **1** is formed first. The second step involves the rearrangement of adduct **1** to intermediate **2** via a cyclic transition structure TS1. The Ca–O bond length shortens from 2.030 Å (in **1**) to 1.916 Å (in **2**), and the C–C bond elongates from a double bond (1.340 Å) to a single bond (1.484 Å).

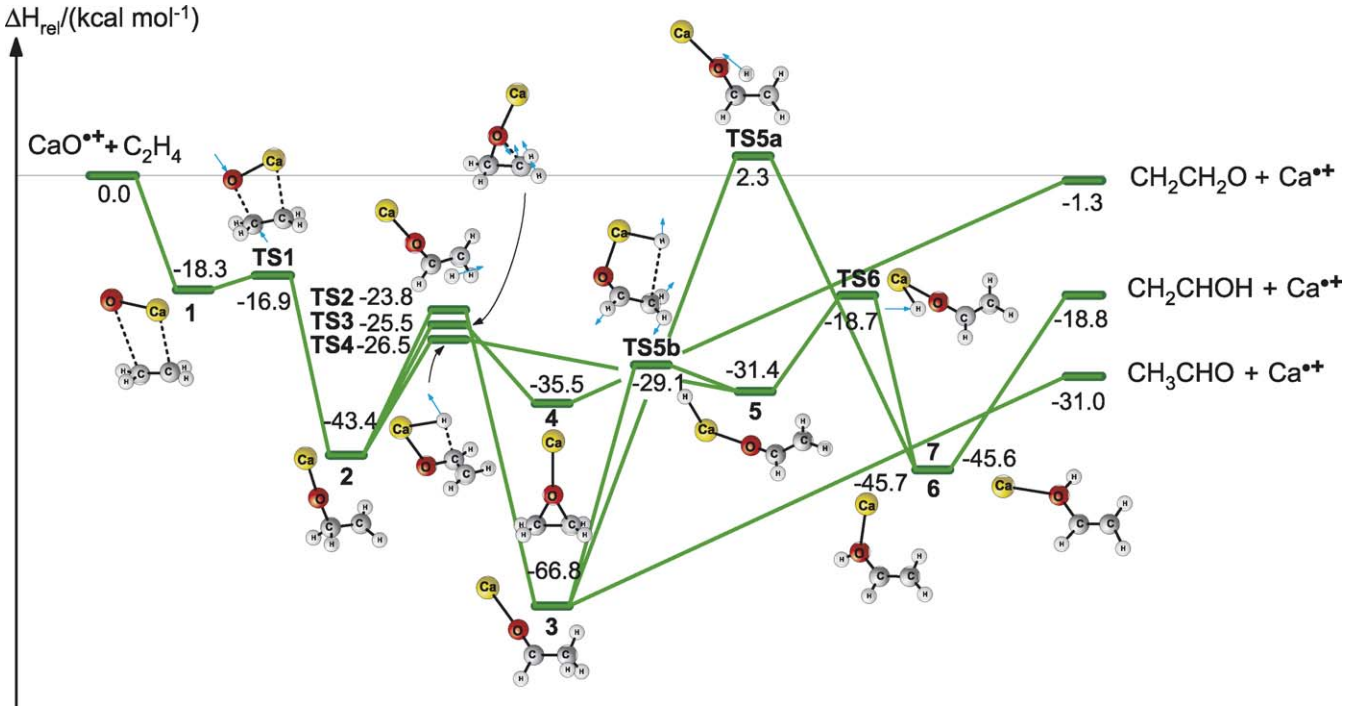

Fig. 4. Potential energy surface for the oxidation of ethylene by $CaO^{\bullet+}$ based on the relative enthalpies computed at the B3LYP/6-311++G(d,p) level of theory.

Intermediate **2** shows a distonic character: the positive charge is mostly located on calcium ($q_{Ca} = 1.46$) and the unpaired electron resides on the carbon atom on the opposite end ($\rho_C = 1.09$). Intermediate **2** can undergo different rearrangement pathways: (i) the covalently bound adduct **2** can undergo a 1,2-H atom shift between two carbons in the CH_2CH_2 moiety, facing a barrier height of 19.6 kcal mol^{-1} (with respect to **2**) and lead to a doublet $(CaOCHCH_3)^{\bullet+}$ (**3**); (ii) it can form a cyclic intermediate (**4**) via TS3 structure, facing a barrier of 17.9 kcal mol^{-1} with respect to **2**, (iii) intermediate **2** can form a stable doublet $(HCaOCHCH_2)^{\bullet+}$ (**5**) by a 1,3-H-atom shift from carbon to calcium over a barrier of 17.0 kcal mol^{-1} with respect to **2**.

4.2.1.1. Formation of acetaldehyde. Fig. 4 shows that acetaldehyde is readily produced when intermediate **2** undergoes a 1,2-H atom shift leading to doublet $(CaOCHCH_3)^{\bullet+}$ (**3**) which can dissociate directly into products $CH_3CHO + Ca^{\bullet+}$.

4.2.1.2. Formation of epoxide. Fig. 4 also shows that epoxide is readily produced when intermediate **2** isomerizes into a cyclic intermediate **4** over TS3 structure. The O–C bond bends toward C–C bond, with the ∠OCC changing from 111.2° to 60.3° from **2** to **4**. In this rearrangement process also a new O–C bond is made and the Ca–O bond elongates by 0.337 Å (2.253 Å). A metallo-cyclic ether $(CH_2CH_2O)Ca^{\bullet+}$ (**4**) dissociates into products, epoxide and bare calcium metal ion. The overall computed exothermicity for the formation of $CH_2CH_2O + Ca^{\bullet+}$ from $CaO^{\bullet+} + C_2H_4$ is 1.3 kcal mol^{-1}.

4.2.1.3. Formation of ethenol. Transformation of **2** to form ethenol is found to be a two-step process and is seen in Fig. 4. A 1,3-H atom shift from carbon to calcium (**2** → **5**) is followed by a 1,2-H-atom shift from calcium to oxygen (**5** → **6**), and then by a release of $Ca^{\bullet+}$. The overall computed exothermicity for the formation of $CH_2CHOH + Ca^{\bullet+}$ from $CaO^{\bullet+} + C_2H_4$ is 18.8 kcal mol^{-1}.

There are two more possible pathways for the formation of ethenol; two of them are shown in Fig. 4:

(i) A 1,2-H-atom shift from carbon to oxygen from **3** to **7** via TS5a, and release of $Ca^{\bullet+}$ to form ethenol. The double O–C bond increases by 0.189 Å, while both Ca–O and C–C bonds shorten by 0.083 and 0.157 Å, respectively. The intermediate **7** has a planar structure, with hydrogen bonded to oxygen on the same side of the double C–C bond, and dissociates into *syn*-CH_2CHOH and $Ca^{\bullet+}$.
(ii) Intermediate **3** can isomerize to **5** over TS5b (which lies 37.7 kcal mol^{-1} above **3**) by 1,4-H-atom shift from carbon to calcium. Further transformation of **5** has already been described.

Finally, our calculations have shown that acetaldehyde can isomerize to *syn*-CH_2CHOH via TS7 by a 1,3-H atom shift from carbon to oxygen (see Supplementary Material for geometries and absolute energies and enthalpies). This isomerization is endothermic by 11 kcal mol^{-1} and has a barrier of 65.9 kcal mol^{-1}. As the H-atom migrates the C–C bond length shortens from 1.504 Å (single bond) to 1.331 Å (double bond). At the same time the C–O double bond (1.206 Å) elongates to a single bond (1.362 Å). Acetaldehyde is found to be more stable then *syn*-CH_2CHOH by 11.0 kcal mol^{-1}.

In addition to this, we have also found that the isomerization of *anti*-CH_2CHOH to the more stable *syn*-CH_2CHOH faces only 3.0 kcal mol^{-1} barrier (with respect to anti-CH_2CHOH) via TS8

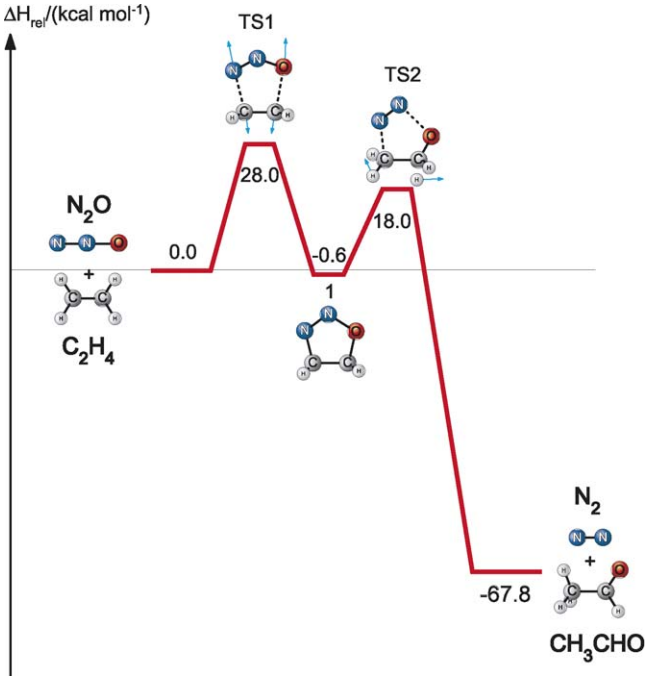

Fig. 5. Potential energy surface for the O-atom transfer from N_2O to ethylene to form N_2 and CH_3CHO based on the relative enthalpies computed at the B3LYP/6-311++G(d,p) level of theory.

(see Supplementary Material for geometries and absolute energies and enthalpies).

4.3. Oxidation of ethylene by nitrous oxide

4.3.1. 1,3-Dipolar cycloaddition of N_2O to C_2H_4

According to the calculations the neutral reaction between nitrous oxide and ethylene proceeds via two-step-concerted cycloaddition pathway. The potential energy surface for the 1,3-dipolar cycloaddition is shown in Fig. 5. Nitrous oxide and ethylene have a parallel plane approach, and a reaction takes place via the transition structure TS1 for addition to form a five-member ring **1**. The formation of two bonds in the transition state TS1 is consistent with a concerted mechanism. Su et al. [15] also have studied the cycloaddition of nitrous oxide with ethylene to form (1) and have obtained similar results at the B3LYP/6-31G* and CCSD(T)/6-311G**//B3LYP/6-31G* levels of theory. The cycloadduct (**1**) dissociates to products CH_3CHO and N_2 over a substantial barrier (TS2) (see Supplementary Material for geometries and absolute energies and enthalpies).

Examination of the single imaginary frequency for TS1 ($476i\,cm^{-1}$) provides an excellent confirmation of the concept of the cycloaddition process. The five-member heteroatom ring **1** is only weakly bound with respect to the reactants (exothermic $-0.6\,kcal\,mol^{-1}$) but is stabilized kinetically by a barrier over TS1. The two new bonds, N–C and O–C, are formed at the same time. All three bonds N–N, N–O, and C–C in a cycloadduct **1** ($H_2CNNOCH_2$) lengthen in comparison to the corresponding bonds in the reactants. We examined the single imaginary frequency for TS2 ($537i\,cm^{-1}$) as well and confirmed that the ring opening and 1,2-H-atom shift between two carbons lead to the final products, acetaldehyde and nitrogen.

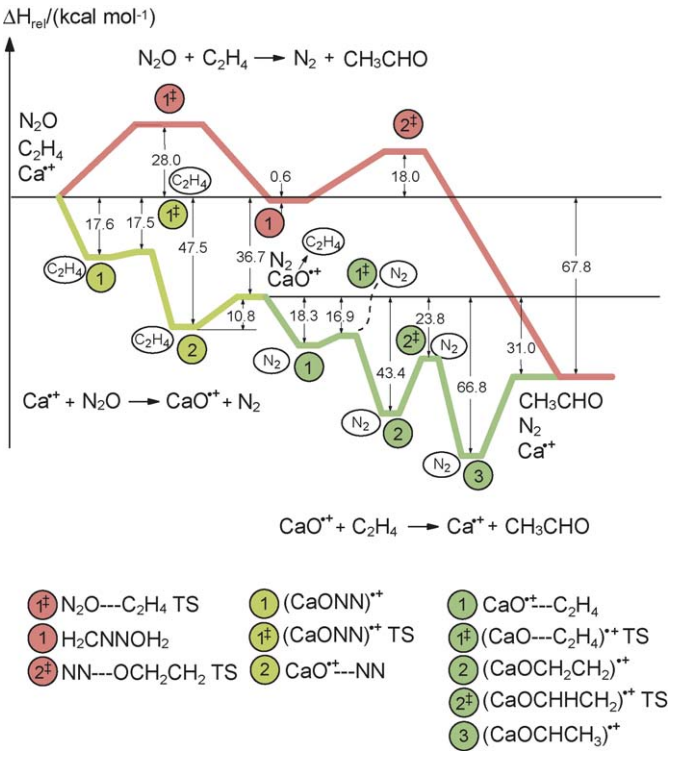

Fig. 6. Enthalpy landscape computed for the oxidation of ethylene with N_2O in the presence and absence of $Ca^{\bullet+}$.

4.4. Enthalpy landscape for catalysis

Fig. 6 provides an overview of the enthalpy landscape for the oxidation of ethylene with N_2O to form acetaldehyde catalyzed by atomic calcium cations.

Clearly the potential energy surface of the ionic route lies below that for the neutral cycloaddition reaction. Furthermore, there are no kinetic barriers to the ionic reaction path. All this is consistent with experimental observations.

4.5. Overview

The "thermodynamic window of opportunity" [5] is a useful thermodynamic indicator of the potential for catalytic activity. $Ca^{\bullet+}$, $Sr^{\bullet+}$ and $Ba^{\bullet+}$ lie in the thermodynamic windows for the

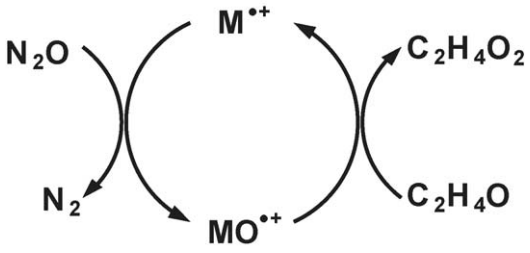

Fig. 7. Generalized catalytic cycle for the homogeneous oxidation of C_2H_4O by nitrous oxide, mediated by atomic metal cations.

Table 3
Thermodynamic windows of opportunity for the catalytic oxidation of three isomers of C_2H_4O and selected alkenes by N_2O

Oxidation	Thermodynamic window[a]	Catalytic ions in the window[b]
$CH_3CHO \rightarrow CH_3COOH$	$40 < OA(M^{\bullet+}) < 122$	All
$CH_3CHO \rightarrow CH_3OCHO$	$40 < OA(M^{\bullet+}) < 105$	All
$CH_3CHO \rightarrow HOCHCHOH$	$40 < OA(M^{\bullet+}) < 94$	All but $Ba^{\bullet+}$
$CH_2CH_2O \rightarrow CH_3COOH$	$40 < OA(M^{\bullet+}) < 150$	All
$CH_2CH_2O \rightarrow CH_3OCHO$	$40 < OA(M^{\bullet+}) < 134$	All
$CH_2CH_2O \rightarrow HOCHCHOH$	$40 < OA(M^{\bullet+}) < 123$	All
$CH_2CHOH \rightarrow CH_3COOH$	$40 < OA(M^{\bullet+}) < 132$	All
$CH_2CHOH \rightarrow CH_3OCHO$	$40 < OA(M^{\bullet+}) < 116$	All
$CH_2CHOH \rightarrow HOCHCHOH$	$40 < OA(M^{\bullet+}) < 104$	All
Propene → acetone	$40 < OA(M^{\bullet+}) < 117$	All
Propene → propanal	$40 < OA(M^{\bullet+}) < 110$	All
Propene → propylene oxide	$40 < OA(M^{\bullet+}) < 87$	All but $Ba^{\bullet+}$
Propene → (Z)-1-propenol	$40 < OA(M^{\bullet+}) < 106$	All
Propene → (E)-1-propenol	$40 < OA(M^{\bullet+}) < 105$	All
Butene → 2-butanone	$40 < OA(M^{\bullet+}) < 116$	All
Butene → butanal	$40 < OA(M^{\bullet+}) < 110$	All
Butene → cyclobutanol	$40 < OA(M^{\bullet+}) < 94$	All but $Ba^{\bullet+}$
Butene → (Z) but-2-en-2-ol	$40 < OA(M^{\bullet+}) < 110$	All
Butene → (E) but-2-en-2-ol	$40 < OA(M^{\bullet+}) < 110$	All

Also included are the group 2 atomic cations that lie within this window.
[a] All values are in kcal mol^{-1} and are taken from Ref. [6].
[b] All refers to the alkaline-earth cations $Be^{\bullet+}$, $Mg^{\bullet+}$, $Ca^{\bullet+}$, $Sr^{\bullet+}$ and $Ba^{\bullet+}$.

catalytic oxidation of ethylene with N_2O by O-atom transfer, as do the low-mass alkaline-earth cations $Be^{\bullet+}$ and $Mg^{\bullet+}$, with O-atom affinities of 86.0 and 55.2 kcal mol^{-1}, respectively [6], that were not measured. The turnover number $N = \phi/(1-\phi)$ is a useful measure of the kinetic performance (efficiency) of a catalyst. Here ϕ is the fraction of the catalytic channel in the reaction cycle ($\phi = \phi_1\phi_2$ if each leg of the cycle is fractionally depleted by competing channels) and N is the number of molecules converted by one catalytic ion. For $Ca^{\bullet+}$, $Sr^{\bullet+}$ and $Ba^{\bullet+}$ the values for N are ≥ 0.22, 0.75, and 0.54, respectively.

All five atomic alkaline-earth cations also lie in most of the thermodynamic windows for the further oxidation of the isomers of C_2H_4O and the oxidation of higher alkenes, with only $Ba^{\bullet+}$ occasionally being an exception (see Table 3).

The generalized catalytic cycle for the further oxidation of C_2H_4O by N_2O is shown in Fig. 7. Table 3 provides the thermodynamic windows for the oxidation of acetaldehyde, ethylene oxide and ethenol to acetic acid, methyl formate, and (Z) ethene-1,2-diol by nitrous oxide. There is some variation in the size of the window according to the isomer that is formed and its enthalpy of formation. All five alkaline earth atomic metal cations fall into these windows with $Ba^{\bullet+}$ being borderline. The window opens somewhat for the higher oxidation compared to the oxidation of ethylene.

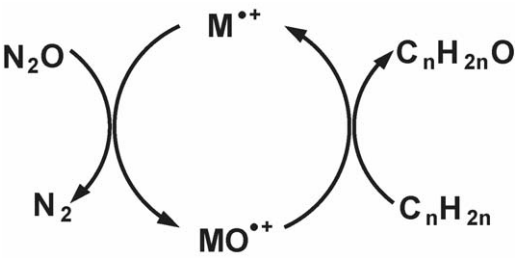

Fig. 8. Generalized catalytic cycle for the homogeneous oxidation of alkenes by nitrous oxide, mediated by atomic metal cations.

The generalized catalytic cycle for the oxidation of other alkenes by N_2O is shown in Fig. 8. Table 3 provides the thermodynamic windows for the oxidation of propene and butene to selected oxides. The size of the window is governed by the enthalpy of formation of the oxide. $Ba^{\bullet+}$ is again somewhat borderline as a catalyst.

The turnover number of both catalytic cycles (Figs. 7 and 8) will be reduced by competing reaction channels in the reduction reaction of $MO^{\bullet+}$ and these may vary in importance depending on the nature of the alkene or the oxide.

5. Conclusions

The catalytic oxidation of ethylene by N_2O has been demonstrated both experimentally and theoretically for $Ca^{\bullet+}$ as a catalyst. The experiments indicate that $Sr^{\bullet+}$ and $Ba^{\bullet+}$ also are catalytic. Formation of CH_3CHO is favorable both kinetically and thermodynamically, although competition with formation of the CH_2CH_2O and CH_2CHOH isomers cannot be ruled out, at least not with $Ca^{\bullet+}$ and $Sr^{\bullet+}$.

Acknowledgements

Continued financial support from the Natural Sciences and Engineering Research Council of Canada is greatly appreciated. Also, we acknowledge support from the National Research Council, the Natural Science and Engineering Research Council and MDS SCIEX in the form of a Research Partnership grant. As holder of a Canada Research Chair in Physical Chemistry, Diethard K. Bohme thanks the Canada Research Chair Program for its contributions to this research.

Appendix A. Supplementary data

Supplementary data associated with this article can be found, in the online version, at doi:10.1016/j.ijms.2006.05.002.

References

[1] J. Smidt, W. Hafner, J. Sedlmeier, R. Sieber, R. Ruttinger, H. Kojer, Angew. Chem. 71 (1959) 176.
[2] G. Tustin, L. Depew, N. Collins, Patent Watch, Chem. Innovat. 31 (3) (2001) 38.
[3] M. Sittig, Handbook of Toxic and Hazardous Chemicals and Carcinogens, 2nd ed., Noyes Publications, Park Ridge, NJ, US, 1985.
[4] U.S. Environmental Protection Agency, Health Assessment Document for Acetaldehyde, EPA/600/8-86-015A, Environmental Criteria and Assessment Office, Office of Health and Environmental Assessment, Office of Research and Development, Research Triangle Park, NC, 1987.
[5] V. Blagojevic, G. Orlova, D.K. Bohme, J. Am. Chem. Soc. 127 (2005) 3545.
[6] Calculated from thermochemical data found in NIST-JANAF Themochemical Tables. http://webbook.nist.gov/chemistry/.

[7] D. Schröder, H. Schwarz, Angew. Chem. Int. Ed. Engl. 34 (1995) 1973.
[8] H. Kang, J.L. Beauchamp, J. Am. Chem. Soc. 108 (1986) 5663;
E.R. Fisher, P.B. Armentrout, J. Phys. Chem. 94 (1990) 1674.
[9] G.K. Koyanagi, V.V. Lavrov, V. Baranov, D. Bandura, S. Tanner, J.W. McLaren, D.K. Bohme, Int. J. Mass Spectrom. 194 (2000) L1;
G.K. Koyanagi, D.K. Bohme, Int. J. Phys. Chem. A 105 (2001) 8964.
[10] G.K. Koyanagi, V.V. Lavrov, V.I. Baranov, D. Bandura, S.D. Tanner, J.W. McLaren, D.K. Bohme, Int. J. Mass Spectrom. 194 (2000) 1;
V.V. Lavrov, V. Blagojevic, G.K. Koyanagi, G. Orlova, D.K. Bohme, J. Phys. Chem. A 108 (2004) 5610;
G.I. Mackay, G.D. Vlachos, D.K. Bohme, H.I. Schiff, Int. J. Mass Spectrom. Ion Phys. 36 (1980) 259;
A.B. Raksit, D.K. Bohme, Int. J. Mass Spectrom. Ion Process. 55 (1983) 69.
[11] M.J. Frisch, G.W. Trucks, H.B. Schlegel, G.E. Scuseria, M.A. Robb, J.R. Cheeseman, V.G. Zakrzewski, J.A. Montgomery Jr., R.E. Stratmann, J.C. Burant, S. Dapprich, J.M. Millam, A.D. Daniels, K.N. Kudin, M.C. Strain, O. Farkas, J. Tomasi, V. Barone, M. Cossi, R. Cammi, B. Mennucci, C. Pomelli, C. Adamo, S. Clifford, J. Ochterski, G.A. Petersson, P.Y. Ayala, Q. Cui, K. Morokuma, N. Rega, P. Salvador, J.J. Dannenberg, D.K. Malick, A.D. Rabuck, K. Raghavachari, J.B. Foresman, J. Cioslowski, J.V. Ortiz, A.G. Baboul, B.B. Stefanov, G. Liu, A. Liashenko, P. Piskorz, I. Komaromi, R. Gomperts, R.L. Martin, D.J. Fox, T. Keith, M.A. Al-Laham, C.Y. Peng, A. Nanayakkara, M. Challacombe, P.M.W. Gill, B. Johnson, W. Chen, M.W. Wong, J.L. Andres, C. Gonzalez, M. Head-Gordon, E.S. Replogle, J.A. Pople, Gaussian'98, Revision A.11.4, Gaussian, Inc., Pittsburgh, PA, 2002.
[12] A.D. Becke, J. Chem. Phys. 98 (1993) 5648;
C. Lee, W. Yang, R. Parr, G. Phys. Rev. B 37 (1988) 785.
[13] C. Gonzales, H.B. Schleger, J. Chem. Phys. 90 (1989) 2154.
[14] T. Su, W.J. Chesnavich, J. Chem. Phys. 76 (1982) 5183.
[15] M.D. Su, H.Y. Liao, W.S. Chung, S.Y. Chu, J. Org. Chem. 64 (1999) 6710.